High Temperature Tribological Properties of Polybenzimidazole (PBI)

Annelise Jean-Fulcrand[1], Marc A. Masen[1], Tim Bremner[2], and Janet S. S. Wong[1*]

[1]The Tribology Group, Department of Mechanical Engineering, Imperial College London, Exhibition Road, London, United Kingdom SW7 2AZ

[2]Hoerbiger Corporation of America Inc., Houston, Texas, USA

[*]Corresponding author: j.wong@imperial.ac.uk

All data and results are available upon requests by email to the corresponding author or tribology@imperial.ac.uk

Abstract: Polybenzimidazole (PBI) is a high performance polymer that can potentially replace metal components in some high temperature conditions where lubrication is challenging or impossible. Yet most characterisations so far have been conducted at relatively low temperatures. In this work, the tribological properties of PBI were examined with a steel ball-PBI disc contact at 280°C under high load and high sliding speed conditions. The dry friction coefficient is relatively low and decreases modestly with increasing applied load. Surface analysis shows that PBI transfer layers are responsible for the low friction observed. *In-situ* contact temperature measurements were performed to provide for the first time direct links between the morphology and distribution of the transfer layer, and the temperature distribution in the contact. The results show that high pressure and high temperature in heavily loaded contacts promote the removal and the subsequent regeneration of a transfer layer, resulting in a very thin transfer layer on the steel counterface. FeOOH is formed in the contact at high loads, instead of Fe_2O_3. This may affect the adhesion between PBI and the counterface and thus influence the transfer layer formation process. To control PBI wear, contact temperature management will be crucial.

Keyword: polybenzimidazole, high temperature, contact temperature, wear, transfer layer

1. Introduction

High performance polymers (HPPs) and their composites are light weight, chemically resistant, thermally stable and self-lubricating, making them good candidates for tribological applications under extreme conditions. These properties allow components made of HPPs to be used in dry sliding conditions where lubrication is not feasible or difficult to be applied. The main limitation of these polymers is the inability to dissipate frictional heat, leading to early component failures. For HPPs such as polyamide-imide (PAI) and polyimide (PI), an increase in the contact temperature above 250°C induces thermal softening and a loss of mechanical strength. Polybenzimidazole (PBI) [1], on the other hand, has a glass transition of 427°C, which makes it a promising candidate for high temperature conditions. It has recently regained potential for tribological applications due to a reduction in manufacturing cost.

Apart from an increased glass transition temperature, PBI also has a higher hardness and modulus than other HPPs. As a results, it has better scratch resistance against a stainless steel indenter at room temperature than polyetheretherketone (PEEK), PI and poly-para-phenylene (PPP) [2]. Under room conditions, PBI also exhibits

better tribological behaviour than PEEK and PAI when it is rubbed against a steel counter [3]. Sharma *et al.* [4] investigated the behaviour of PBI under a range of loads and temperatures (100 – 200°C) and found the coefficient of friction to be fairly independent of load until a limiting pressure-velocity (PV) value is reached, after which the coefficient of friction drops. The PV value is the product of average contact pressure (P) and sliding speed (V) and is often used as a measure of the amount of frictional heat generated during rubbing [5-8]. The observed drop in coefficient of friction after a PV limit is reached is attributed to frictional heating and the subsequent softening of the polymer at the rubbing interface. Note, the PV limit for PBI decreases as the temperature increases [4], highlighting that the PV limit is not a material property and can change depending on operating conditions.

The effects of load on the friction and wear performance of polymers have widely been investigated [9-12], but results are highly dependent on the type of polymers and the applied load range. Briscoe *et al.* [13-15] and Zhang *et al.* [16] showed that applied load affects the deformation mechanisms of polymers such as PEEK, polycarbonate (PC), polyethylene and poly(methyl methacrylate) (PMMA) in a contact. At low loads, amorphous polymers such as PMMA, PC and polystyrene display viscoelastic behaviour, until the applied load reaches a critical load after which plastic deformation and fracture may occur. In the case of PI and PAI, Yanming *et al.* and Unal *et al.* [13, 14] observed a decrease in coefficient of friction and wear rate with increasing load at room temperature. The effect of bulk temperatures up to 300°C was investigated for PI [13, 15]. When the bulk temperature of PI reaches 200°C, a significant increase in wear rate and a reduction of the friction coefficient are observed. Lancaster [16] observed that the wear rate for amorphous polymers is at its lowest just before the glass transition and then sharply increases. The severe wear produced above a critical temperature is associated with adhesive wear at the interface [17]. Good adhesion of the polymer to the countersurface favours the formation of a transfer layer [18, 19]. However, it is not always an assurance of low wear of the polymer [18]. These results highlight that both load and temperature strongly impact on the tribological properties of polymers, which is likely due to their effects on the process of material transfer and the properties of the transferred material.

The self-lubricating ability of polymers is frequently attributed to the formation of a so-called transfer layer when polymers are rubbed against steel countersurfaces [20]. However, the concept of a 'transfer layer' is ill-defined and is usually characterised in term of thickness, coverage and homogeneity. An efficient transfer layer is commonly described as a "thin," "uniform," and "stable" layer of material that has been transferred from one surface to another by adhesive wear [21]. Transfer layer formation is often related to thermal softening of the polymer and polymer molecular structure (alignment) [22]. The connection between the occurrence of a transfer layer and wear of the polymer in a polymer-steel system has been widely studied [18, 23-26]. However, no generic model exists that can be used to accurately predict wear [27, 28]. Indeed it is difficult to establish relationships between transfer layer properties and wear rate as both are highly dependent on polymer structure, surface roughness, interactions between rubbing surfaces, and test conditions.

High performance polymers such as PEEK [26, 29], PI [13] and polyamide (PA) [23] have rigid backbones and form 'lumpy', uneven transfer layers on the countersurface. Laux and Schwartz [26] showed that the PEEK

transfer layer coverage on steel and PEEK wear volume increase with contact pressure. However, no correlation was observed between the thickness of the transfer layer and the volume of wear of the polymer. For PI, the amount of polymer transfer increases with either normal loads or bulk temperatures of the material [28, 30-32]. In addition, the morphology of the transfer layer is temperature dependent. At 25°C, the transfer layer generated by PI is coarse and patchy whilst above 100°C it is thin and drawn out, leading to a decrease in wear rate. Transfer layer formation is also dependent on the frictional heat generated; *in-situ* thermography techniques [33-35] have been used to examine the temperature distribution within tribological contacts and to correlate it to the transfer layer morphology and thickness.

The maximum functional working temperature of HPPs depends on their glass transition temperatures, T_g. For example, PAI, which has a $T_g = 280\,^{o}$C, shows good performance at temperatures up to 250°C. PBI, having a T_g of 427°C, has shown promising performance at high pressures under non-lubricated conditions at a similar temperature range [3]. However, so far no work has been conducted to verify the performance of PBI at higher temperatures. The objective of this study is to understand the effect of load on the tribological behaviour of PBI at high temperatures. PBI specimens were tested at temperature of 280°C and contact pressures up to 56 MPa. Due to the potential impact of transferred materials on friction and wear of polymers [21, 36], we aim to provide insights on how applied load influences the materials transfer process. It is hypothesized that severe conditions as well as elevated temperatures should promote the formation of a polymeric transfer layer on steel counterface [24, 31]. The tribological properties of the PBI-steel system were investigated by characterising the wear behaviour of the polymer as well as the formation of the transfer layer onto the countersurface. *In-situ* IR thermography of PBI-sapphire contacts was used to estimate frictional heat generated during rubbing. The temperature distribution inside the contact was related to transfer layer development.

2. Materials and Method

2.1. Materials

PBI specimens in the form of discs and balls (provided by Hoerbiger America Inc.) were made by compression moulding using Celazole U-60 (PBI Performance Products, Inc.). The PBI discs have a diameter of 46 mm and a thickness of 5 mm with an average roughness R_a of 1.41 ± 0.43 µm, while the PBI balls, with diameter of 6 mm have a roughness of about 1.6 µm. AISI 52100 bearing steel balls of 6 mm diameter and a surface roughness R_a below 10 nm were supplied by PCS instruments. The mechanical and thermal properties of PBI and steel are listed in Table 1. PBI discs and balls were wiped with isopropanol and dried in an oven at 150°C for at least 2 days [37]. Steel balls were cleaned using toluene in a sonication bath for fifteen minutes followed by sonication in isopropanol (IPA) for another five minutes and were dried using a dry cloth.

Bare sapphire discs and aluminium coated sapphire discs were used for the contact temperature measurements. Sapphire discs were cleaned using isopropanol and sonicated for 15 min. Aluminium coated sapphire discs were wiped with isopropanol.

Table 1: Material properties of ball and disc samples

	Glass transition temperature Tg (°C)	Thermal conductivity (W/mK)	Heat deflection temperature (°C)	Compressive yield strength (MPa)	Young's modulus at 20°C (GPa)	Roughness (µm)
PBI U-60	427*	0.3*	435*	370* at 20°C	5.9*	Ball: 1.6
				120* at 280°C		Disc: 1.41 ± 0.43
				50* at 375°C		
Steel 52100	N/A	46	N/A	2500	200	0.01
Sapphire	N/A	24	N/A	2068	380	< 0.01
Aluminium coating	N/A	205	N/A	N/A	73	0.006 ± 0.0002

* Data from PBI Performance Products

2.2. Tribological characterisations

Friction measurements were conducted using a High Temperature Tribometer (Anton Paar TriTec, Switzerland). A sphere-on-flat geometry was used where a stationary ball was loaded against a rotating disc using a dead weight. Frictional force was obtained by the amount of deflection of a flexure arm attached to the ball measured by a displacement transducer. A heating element located around the disc heated the sample to the pre-set temperature. The test chamber was thermally insulated to minimise temperature fluctuations and heat losses. The surface temperature of the disc was 280°C as monitored by thermocouples located below and above the disc. In this study, rotating PBI discs were rubbed against stationary steel balls under dry sliding conditions, i.e. no lubricant was used. The applied normal loads ranged from 3 to 12 N and the sliding speed was fixed at 2 $m \cdot s^{-1}$. While the usefulness of PV values may be questioned, and PV values are ill-defined for a sphere-on-flat geometry used in our tests, it was calculated based on the initial average pressure and ranged between 75 and 119 $MPa \cdot m \cdot s^{-1}$. As rubbing progressed, a steady state was reached where the coefficient of friction plateaued. The steady state PV values (40 – 80 $MPa \cdot m \cdot s^{-1}$) was lower than the initial PV values as contact area increased due to wear of the disc and the ball. Note that these values exceed the PV values commonly studied, which typically are about 3 – 7 $MPa \cdot m \cdot s^{-1}$ [4]. This means that in this work, the PBI specimens were exposed to very severe operating conditions. Each test lasted for a total of 30 minutes, or 3600 metres sliding distance. The coefficient of friction changed during the initial running-in period and the duration of this running-in period varied among samples. This is due to variations in surface finishes among different samples, but it has no effect on the steady state coefficient of friction. After the initial running in period, the coefficient of friction stabilised when the steady state regime was reached. The reported coefficients of friction in this work are those measured during this steady state and were similar among repeated experiments. Friction tests were also conducted with PBI disc-PBI ball contacts and results compared to those obtained with PBI disc-steel ball contacts.

The friction results presented are average values of at least three repeated experiments, and the error bars represent standard deviations of the collected steady state (average) friction coefficient values.

2.3. Wear and Surface characterisations

During the friction tests, both PBI disc and steel ball were worn. The worn surfaces were observed with optical microscopy (Hirox RH-2000 with a MXB-2500REZ objective). The topography of worn surfaces was also examined using white light interferometry (Wyko NT9300, Veeco Metrology, USA) with a height resolution of 0.1 nm. Wear tracks were formed on the PBI discs (see Figure 1(e) – 1(g)). The wear volume of each PBI disc was estimated by measuring the cross-sectional area of the wear track (see Figure 1(b) – 1(d)) and multiplying it by its length. The cross-sectional area of the wear track was measured at three locations on each wear track and averaged.

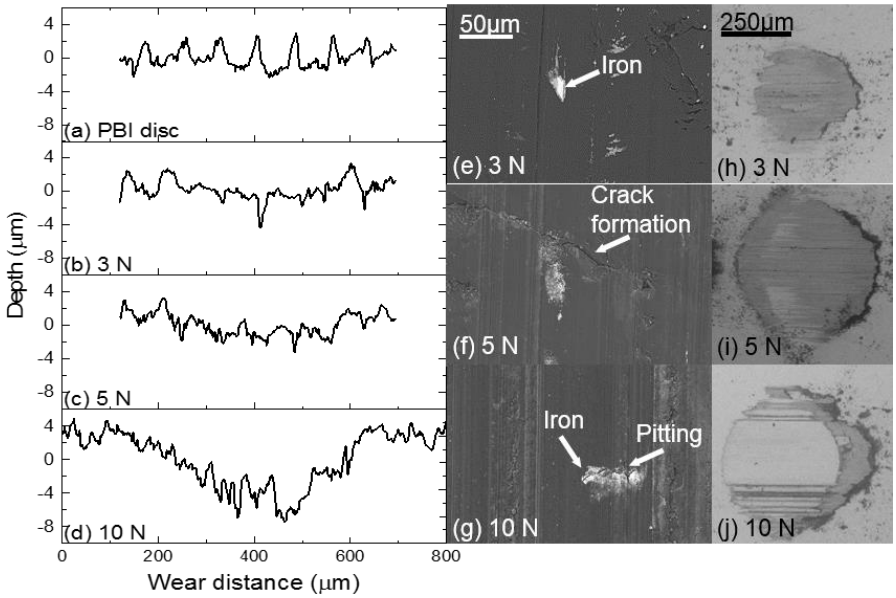

Figure 1 (a) Pristine PBI disc profile; (b) – (d) PBI wear track profiles orthogonal to the rubbing direction; The SEM micrographs of (e) – (g) wear tracks on PBI discs and (h) – (j) wear scars on steel balls using a BSE detector at various loads.

Flattened regions (see Figure 1(h) – 1(j)), called wear scars, with a diameter of approximately a few hundreds μm, developed on the steel balls where they rubbed against the PBI disc. It was observed that the wear scar was covered by a thin polymeric layer (< 1 μm) transferred from the PBI disc. This transfer layer is seen in Figure 1(h) – 1(j) as dark grey material. The wear volume of each steel ball was obtained from the surface topographic image of the wear scar and its surroundings. The raw images were background corrected with the nominal profiles (6 mm diameter) of the steel ball, as such the wear volume of the ball appears as a negative volume. The morphology of the transfer layer on the steel ball wear scars was obtained by flattening raw height images of wear scars with straight line background correction.

Worn steel ball and PBI disc surfaces were also examined using the backscattered electron (BSE) mode of a scanning electron microscope (SEM) at 10 kV energy (Hitachi S-3400N, Hitachi High-Technologies, Japan). The energy dispersive X-ray (EDX) mode of the SEM and X-ray Photoelectron Spectroscopy (XPS) (Thermo Scientific K-Alpha+ X-ray photoelectron spectrometer) were used to obtain chemical information of pristine PBI discs, cleaned steel balls and steel ball wear scars. The depth resolutions of EDX and XPS are 1 μm and 20 nm respectively. For XPS, samples were mounted using conductive carbon tape and an Argon flood gun was used to avoid sample charging. XPS spectra were recorded at an operating pressure of 2×10^{-9} mbar and at 20 eV pass

157 energy for core level spectra (C 1s, O 1s, N 1s and Fe 2p) with an X-ray spot size of 200 μm^2. Avantage software
158 package from Thermo Scientific was used to analyse the spectra.

159 2.4. Contact temperature rise measurement

160 The contact temperature is defined as the temperature at the rubbing interface, which can be substantially
161 different from the ambient temperature of the test due to frictional heating. To qualitatively show the general
162 trend of temperature rise with test conditions and possibly heat distributions in tribological contacts involving
163 PBI, *in-situ* contact temperature measurements were performed with Infrared (IR) thermography. To implement
164 IR thermography, the disc needs to be IR transparent. As a result, the steel ball-PBI disc contact for friction
165 measurements cannot be employed. Taking advantage that sapphire fully transmits IR radiation in the
166 wavelength range of 3 – 5 μm, the test configuration for these temperature measurements was changed to a
167 stationary PBI ball against a rotating sapphire disc. It needs to be noted that, due to differences in thermal
168 conductivity, the actual heat profiles in this stationary PBI ball-rotating sapphire disc contact is likely different
169 from that of the stationary steel ball-rotating PBI disc contact used in the friction tests.

170 To measure the temperature increase in the contact, a stationary PBI ball was loaded against a rotating sapphire
171 disc from the bottom with an EHL rig (manufactured by PCS instrument). An infrared camera (X6540SC, FLIR)
172 was placed above the contact to capture IR irradiation emitted during rubbing. The camera has a 320 × 256
173 focal plane array. With a 5× lens, it has a lateral resolution of 6.3 μm. During rubbing, IR radiation came from
174 both the rubbing interface and the bulk of the sapphire disc. To obtain the contact temperature, calibrations
175 were performed to remove the IR contribution from the latter. Details of the technique and the calibration
176 process are described in [33, 35]. The setup does not allow tests to be conducted at elevated temperature,
177 hence all contact temperature rise measurements were conducted at 25°C.

178 3. Results and Discussion

179 3.1. Effect of load on tribology of PBI

180 The tribological properties of PBI at 280°C are shown in Figure 2. Steady state friction coefficients, μ, as a
181 function of applied normal load W are presented in Figure 2(a). The variation of the steady state friction among
182 repeated experiments are reflected by the error bars. Such variations are inherent to dry sliding tests and are
183 deemed acceptable. For steel ball-PBI disc contacts (open circles, Figure 2(a)), μ decreases marginally as W
184 increases. However due to the intrinsic variability in dry friction tests, such effect is considered to be small.
185 Note μ for steel ball-PBI disc contacts and PBI ball-PBI disc contacts (open circles and solid squares respectively,
186 Figure 2(a)) are similar at low loads. A PBI ball-PBI disc contact has a lower μ (0.08) than that of a PBI-steel
187 contact (0.13) at $W = 10$N. This is probably due to poor thermal conductivity and lower shear strength of PBI.
188 With a quicker drop in contact pressure (due to wear) and higher contact temperature as compared to a PBI-
189 steel system, it is not surprising that the friction of a PBI-PBI system is lower.

190

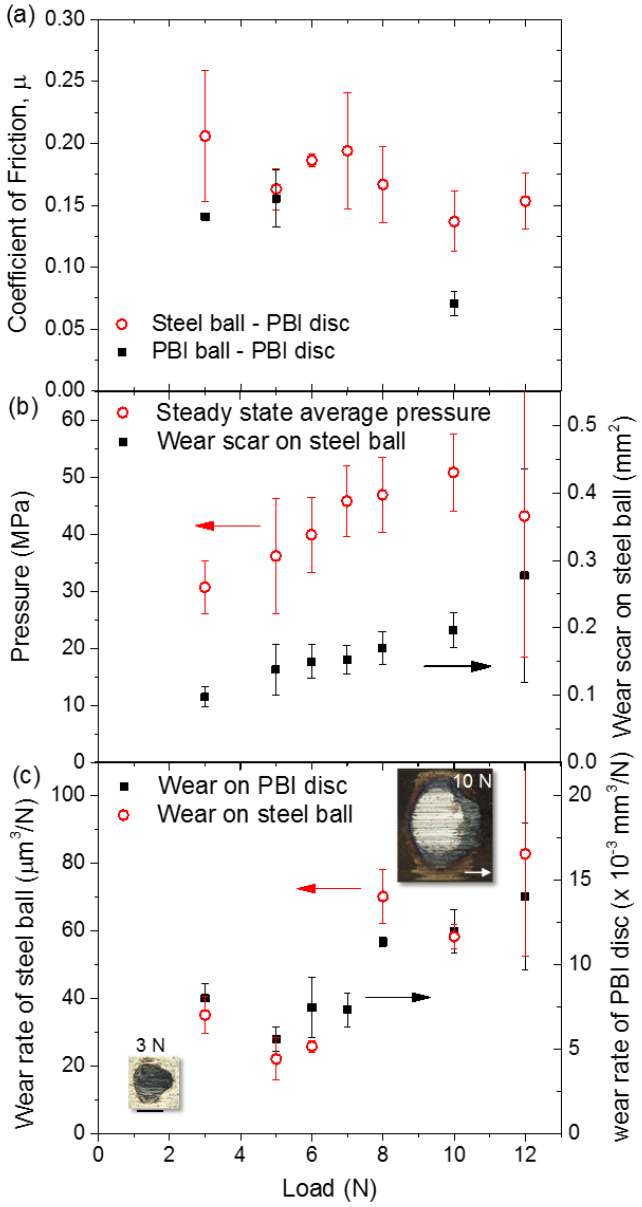

Figure 2: (a) Steady state friction coefficient μ of steel ball-PBI disc and PBI-PBI contacts; (b) area of the steel ball wear scar and the steady state pressure of the steel ball-PBI disc contacts; (c) wear rates of PBI disc and steel ball; Insert: micrographs show steel ball wear scars at the end of the friction tests at 3 and 10 N. The white arrow shows the sliding direction and the black scale bar corresponds to 200 μm.

Wear scars on steel balls were examined with optical microscopy, scanning electron microscopy and white light interferometry. It is noted that the shape of the wear scar changes from circular at low loads to elliptical at higher loads, with the major axis orthogonal to the rubbing direction (see the picture inserts in Figure 2(c)). At low loads, the shape of the contact is approximately circular as the material behaves elastically. With increasing load, the stress distribution inside the contact changes as a result of increased shear stress, meaning the maximum stress shifts towards the leading edge of the contact. Additionally, viscoelastic behaviour of the PBI results in a delayed recovery of the material after the contact has passed, causing an elliptical contact area [38, 39].

As the steel ball wears during the experiment the apparent contact area between the two materials increases (solid symbols, Figure 2(b)), leading to a reduction of the average contact pressure. From the measured area of the wear scars, the steady state average contact pressure P_{ave} can be estimated. The obtained values are shown as open circles in Figure 2(b). The steady state contact pressure increases with increasing load until it reaches a plateau at 40 to 50 MPa when $W > 7$ N. These results suggest that the contact area increases with increasing load up to a critical failure stress of approximately 40 MPa. As a first order approximation, the shear strength τ relates to the compressive strength σ as $\tau \sim \frac{1}{\sqrt{3}}\sigma \approx 0.6\sigma$. Note the compressive yield stress σ_y of PBI at 280°C is about 120 MPa, which reduces to 50 MPa at 375°C (see Table 1). This means that 40 MPa is a reasonable value for the failure stress σ_f as the temperature increase in the contact due to frictional heating may be substantial in our tests. The contact temperature rise is further discussed in section 3.3.2.

The wear rate of PBI discs (solid squares) and steel balls (open circles) are presented in Figure 2(c). Both sets of results show a stepped increase in wear rate at $W = 7$ N. Results in Figures 2(b) and 2(c) suggest that the deformation regime has changed from mainly elastic deformation (low loads) to plastic deformation (high loads) when the contact pressure reaches the critical failure stress of PBI. This is supported by the morphology of the wear tracks on the PBI discs shown Figure 1). The surface of the PBI wear tracks appears to be '*ironed*' at $W = 3$ N (Figure 1(e)), giving rise to a smoother surface in the wear track (Ra ~ 0.1 μm) than that of a pristine disc (Figure 1(a) Ra ~ 1 μm). The corresponding PBI wear track profile orthogonal to the rubbing direction (Figure 1(b)) shows mild deformation with a maximum track depth of about 0.8 μm. As the applied load increases such that P_{ave} approaches σ_f, new surface features are found within the PBI wear tracks. At $W = 5$ N (Figures 1(c) and (f)), cracks form on the wear track. When $W > 5$ N, grooves as deep as 4 μm are observed along the entire wear track (Figure 1(d)). The number, the width and depth of grooves, as well as the roughness of the wear track increase with load (compare Figures 1(d) and (g)). An increased number of cracks and pitting zones appear on the PBI discs at higher loads, leading to an increase in material removal as observed by a deeper wear track in the polymer and an increase in debris accumulation around the contact and in the test chamber. At the same time, more iron-rich debris, appearing white in Figures 1(e) – (g), is found on the surface of the PBI, see also section 3.2 for details. This debris originates from the steel ball during rubbing, may be work hardened and embeds in the polymer, resulting in potentially further (abrasive) wear of the steel ball.

During sliding polymeric material was transferred from the disc to the surface of the steel ball (the dark grey/black regions in the SEM micrographs, Figures 1(h) – (j)). The applied load affects the morphology of these polymeric transfer layers. Up to $W = 5$ N (Figures 1(h) and 1(i)), the transfer layer almost completely covers the wear scars, although the layer is not uniform. An accumulation of polymer is observed at the trailing edge of the contact, which increases with increasing load. Streaks of polymer are seen across the wear scar, running parallel to the sliding direction. As the load increases further (Figure 1(j)), the transfer layer thickness decreases and the majority of the wear scar appears light grey. Note that light grey regions in the SEM micrographs are regions of high electron density and thus suggests those regions are steel. However, a very thin polymeric layer may still exist.

3.2. Characterisation of Polymeric Transfer Layer

The morphology of the transfer layers on the surface of the steel balls was examined with interferometry. Two typical measurements obtained are shown in Figures 3(a) and 3(b) for $W = 5$ and 12 N respectively. As the load increases, the size of the wear scar increases. In both cases, the surface topography is not homogeneous and material has accumulated at the trailing edge. Figures 3(c) and 3(d) show the surface profiles of only the wear scars along the sliding direction, marked as the dashed lines in Figures 3(a) and 3(b). In these graphs any deposits at the inlet and outlet, i.e. outside the wear scar, are excluded. Figure 3(c) shows the profiles for low loads, W = 3 and 5 N, whilst Figure 3(d) gives profiles from $W = 10$ and 12 N. Due to the heterogeneous nature of the layer, its thickness varies, however, at loads $W < 7$ N, the surface is covered by a rather thick transfer layer. When $W > 7$ N, the layer is thinner and steel may be exposed. The insert in Figure 3(c) shows the amount of materials accumulation outside of the wear scar increases with increasing loads.

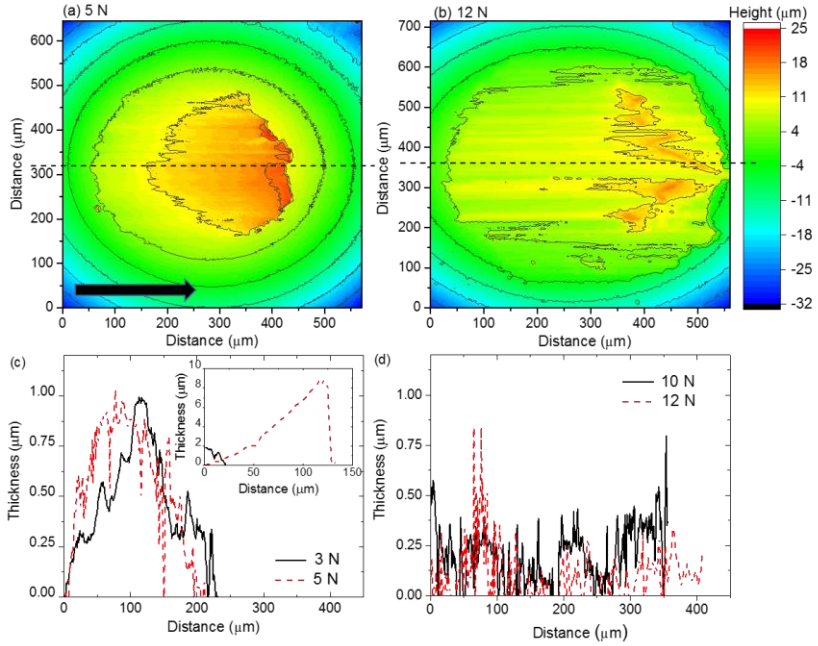

Figure 3 (a) and (b) Morphology and (c) and (d) thickness profiles of transfer layers on wear scars of steel balls. The arrow shows the sliding direction. Area around the scars appear lower in (a) and (b) due to the curvature of the ball. The dashed lines show where the thickness profiles are obtained. The insert in (c) shows the profile of polymeric accumulations at the outlets of the contacts.

Information on the chemical compositions of a cleaned steel ball, a pristine PBI disc and at various regions in steel ball wear scars were obtained with EDX (see Figure 4). Note the amount of an element is expressed in atomic percentage (i.e. the number fraction). The pristine PBI samples are composed of 96% carbon and 4% oxygen, with no detectable iron on the surface. The cleaned steel ball contains 76% iron and 24% carbon. The amount of carbon present on the cleaned steel surface is high due to the use of isopropanol in the cleaning procedure. The isopropanol layer will have no effect on the friction results as it will be remove during rubbing.

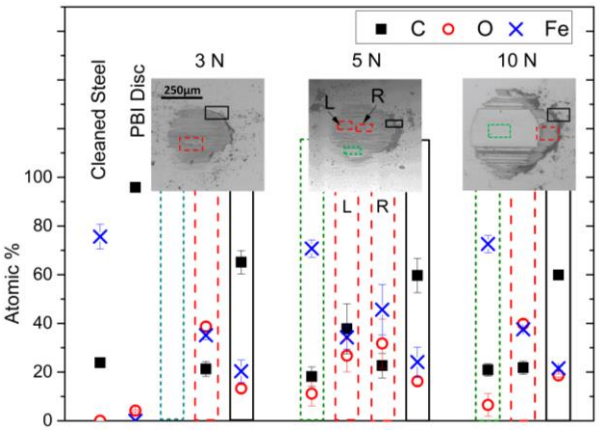

Figure 4 Chemical information of steel ball wear scar surfaces using EDX analysis

Based on the SEM micrographs of steel ball wear scars, two regions can be identified (see Figure 4). This is best illustrated by the wear scar obtained at $W = 5$ N. The majority of the wear scar is grey in colour (dashed boxes, labelled 'L' and 'R', 5 N). These regions have an iron content of about ~40 – 50%, although the actual amount of iron varies. There are also regions that appear light grey (dotted box, 5 N). These regions have an even higher iron content of approximately 70%, similar to that of a cleaned steel ball. Moving towards the trailing edge on the right hand side, a slightly darker region is followed by a line of black deposit (solid line box, 5 N) at the outlet, which has a very low iron content (~20%). Similar grey regions with similar iron contents (40 – 50% iron) are found in the wear scars formed at lower load (see results for 3 N, Figure 4). No light grey region is observed in this case. For $W = 10$N, the majority of the wear scar is light grey, with very high iron content (~70%). These results suggest that the grey scale of these SEM micrographs of wear scars correlates with the thickness of the polymeric material, with darker colour corresponding to a thicker layer and hence a reduced iron signal. They are consistent with results shown in Figure 3 that the polymeric layer coverage and layer thickness in the wear scar decrease with increasing applied load. Note the wear scar has a higher oxygen content (circles, Figure 4) than the cleaned steel ball. The wear scars formed at low loads (grey from 3 N and 5 N, Figure 4) have higher oxygen content than those formed at high loads (light grey from 10 N, Figure 4). This may be due to differences in oxide thickness, or oxides' chemical structures.

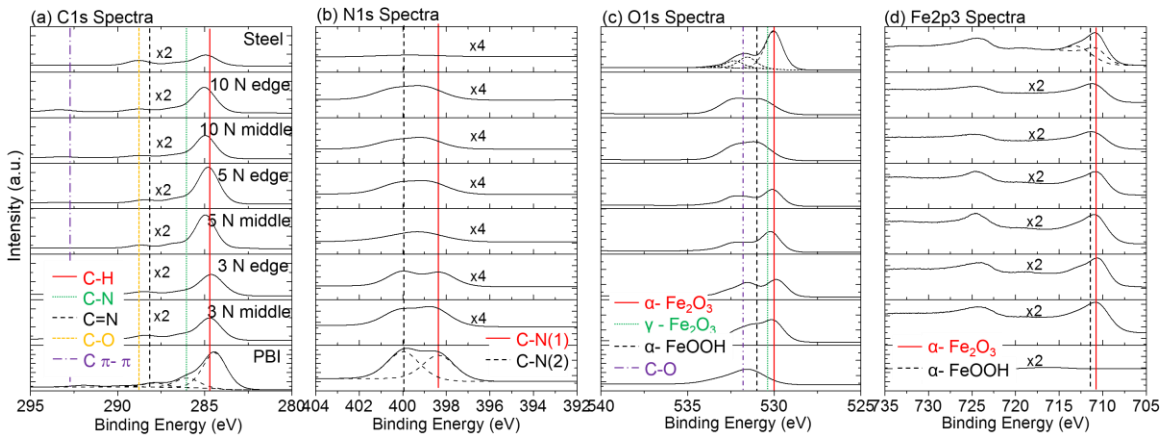

Figure 5 XPS spectra revealing the surface chemistry of cleaned steel ball, pristine PBI disc, and steel ball wear scars produced at various loads. 'Middle' and 'Edge' in the legends show the locations the spectra were taken, being near the middle and the trailing edge of wear scars respectively.

The surface chemistry of the wear scars on the steel balls can be better delineated with XPS, a technique that is sensitive to the top 10 nm of the surface. Spectra obtained on steel ball wear scars are compared to those from the cleaned steel ball and the pristine PBI disc. For the C1s spectra (Figure 5(a)), even with pristine PBI, the dominant signals are from the C-H stretch, which is common in contaminants and aliphatic carbon. The other C1s bands related to imidazole and chemisorbed imidazole [40] are weak. Focusing on N1s spectra (Figure 5(b)), the two C-N stretches with binding energy of 396.6 and 400.4 eV, distinguishable from the pristine PBI spectrum, are also observed from spectra obtained in the steel ball wear scars. Note, no signal in this range is detected on the cleaned steel surface. This confirms that the transfer layer observed in the wear scars (see Figures 3 and 4) are composed of PBI. Among those spectra from the wear scars, the two C-N peaks are most distinguishable for $W = 3$ N since it has a thicker layer and thus gives clearer spectral features. Note, these two C-N peaks are, although weak, also observed at $W = 10$ N, confirming that a very thin PBI layer exists in the centre of the wear scar obtained at high loads as suggested by results from the SEM micrograph (Figure 1(j)) and the EDX results (Figure 4). The combination of these XPS results and the surface profile of the layer as shown in Figure 3(d), suggest that the layer is not uniform and is thin (an average thickness of about 200 nm). In Figure 2, it was shown that the friction is independent of the applied load, whilst the thickness of the developed transfer layer is highly dependent on load. The results here thus suggest that the existence of the transfer layer, rather than its thickness, governs the observed friction.

The iron oxide found on the cleaned steel ball is α-Fe_2O_3 (530 eV, Figure 5(c)). This is not observed in the EDX analysis (Figure 4) probably because the oxide layer is very thin (a few nm, confirmed by ellipsometry measurements, results not shown). The α-Fe_2O_3 peak is also clearly identified in the spectra of the wear scars produced at $W = 3$ and 5 N (Figure 5(c)). The fact that oxides are detected in the wear scars by both XPS and EDX suggests that firstly the conditions in the rubbing steel ball-PBI disc contacts promote the formation of oxides. Secondly, the transfer layer is locally patchy, i.e. oxides underneath the layer are exposed and interact with the X-ray beam directly; or iron oxides are dislodged from the steel ball and debris was embedded into the transfer layer.

An increase in applied load to $W = 10$ N changes the type of oxides in the wear scar to α-FeOOH as shown in Figure 5(c) and (d) by the appearance of the O1s peak at 531.4 eV and the Fe2p peak at 711.9 eV. This is intriguing because α-Fe_2O_3 is the stable oxide form at 280°C [41]. Below 570°C Fe_3O_4 can also form whilst above 570°C FeO dominates. The formation of the observed α-FeOOH would require hydrolysis of the oxides. PBI is known to absorb water [42, 43]. While PBI discs used in this study have been dried, it is likely that only water locked in PBI at and near the disc surface was removed. As the load increases, the PBI disc is increasingly worn, such that PBI originally located deep below the surface (see Figure 1 where the depth of the centre of disc wear track is about 7 μm), which might still hold a relatively large amount of water, is exposed. This newly exposed PBI can interact with the freshly exposed steel of the wear scar and as a result α-FeOOH may be formed. The results also suggest that rubbing may have promoted such a reaction. However, more work is required to understand how the rubbing process gives rise to the formation of various oxides.

3.3. Materials transfer process

3.3.1. Transfer layer formation

Materials transfer may influence the tribology of steel-PBI contacts. Results presented in sections 3.1 and 3.2 suggest that operating conditions play a significant role in determining the final morphology of the transferred materials. In this section, we investigate the materials transfer processes and the role of the applied load.

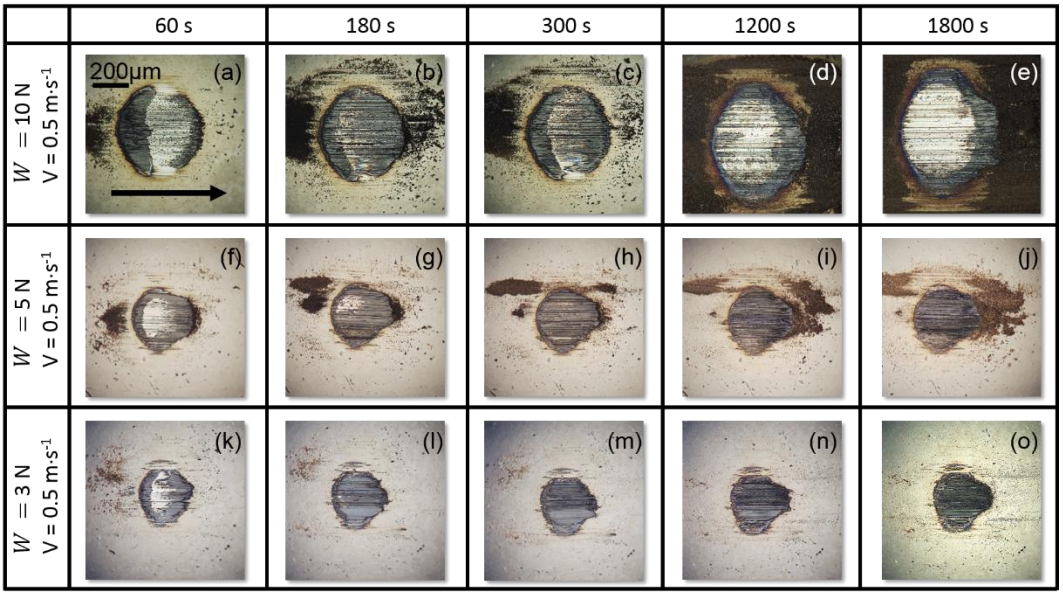

Figure 6 PBI transfer layer formation on steel wear scars at different rubbing time at 280°C (a) – (e) 10 N; (f) – (i) 5 N; (k) – (o) 3 N.

Images showing how wear scars on steel balls evolved during rubbing at various applied loads are presented in Figure 6. Note the dark grey materials are polymeric as shown in section 3.2. At $W < 7$ N, the steady state pressure is lower than σ_f. While PBI wear tracks show minor ironing at low loads (see Figures 1(b) and 1(e)), the steel ball wear scars are nevertheless completely covered by polymeric materials by the end of the test (see Figure 1(h)). The amount of PBI transferred to the steel wear scars increases with time, starting at the leading edge (left) of the scars. Polymeric material also starts accumulating at the trailing edge (right) and behind it (see

Figures 6(f) and 6(k)). The centre of the wear scars appear white, suggesting that there is little transferred material. The area covered by the polymer increases as rubbing proceeds, propagating from the trailing edge (right) to the leading edge (left) (see Figures 6(k) – 6(m) and 6(f) – 6(h) for $W = 3$ and 5 N respectively). Eventually the whole wear scar is covered by a non-uniform polymer transfer layer. The time it takes for a complete polymeric transfer layer to form depends on the applied load, with shorter times corresponding to lower loads.

Figures 6(a) – (e) show images obtained at $W = 10$ N, where σ_f is reached. As rubbing proceeds, the contact area increases from 0.22 to 0.32 mm^2. Similar to what was observed for the low load cases, material transfer occurs at the very early stage of rubbing. After 60 s of rubbing, transferred material is mainly deposited near the leading and trailing edges (Figure 6(a)). Shortly, most of the scar is covered by a transfer layer that has developed from the trailing edge (Figure 6(b)). After 1200 s of rubbing, polymeric material also accumulated at the inlet (left) and the outlet (right) of the contact (see Figures 6(d) – (e)), whilst the wear scar itself appears white, suggesting little transfer of polymer at the contact (see also Figure 4). There is a grey crescent-shaped region of polymeric deposition at the outlet of the contact. Once such a two-zone morphology is formed (Figure 6(d)), it remains qualitatively the same throughout the rest of the test, while the white region slightly grows with time. Interestingly the stabilisation of the two-zone transfer layer morphology coincides with the stabilisation of the coefficient of friction. Note an increasing amount of polymeric materials accumulates around the wear scar with continued rubbing.

3.3.2. Contact temperature during rubbing

The results presented so far show that at low loads, where the steady state applied pressure P_{ave} is less than the critical failure stress of PBI σ_f, the steel ball experiences mild wear that is not sensitive to the applied load and the wear scars are covered by the polymer. When P_{ave} is above σ_f, the steel ball wears severely and the wear scar is mostly bare. At the same time, the amount of wear from the PBI disc is high and increases with the load. In all cases, a crescent shaped polymeric deposit region forms near the trailing edge of the wear scars. All these suggest a link between the morphology of the polymer transfer layer on the steel balls and the friction and wear of the steel ball-PBI disc contacts. We believe that frictional heating is the link. The increase of the temperature inside the PBI ball-sapphire disc contact was measured at room temperature by IR thermography as described in section 2.3. Results are presented in Figure 7 (temperature maps) and Figure 8 (average and maximum temperature increase).

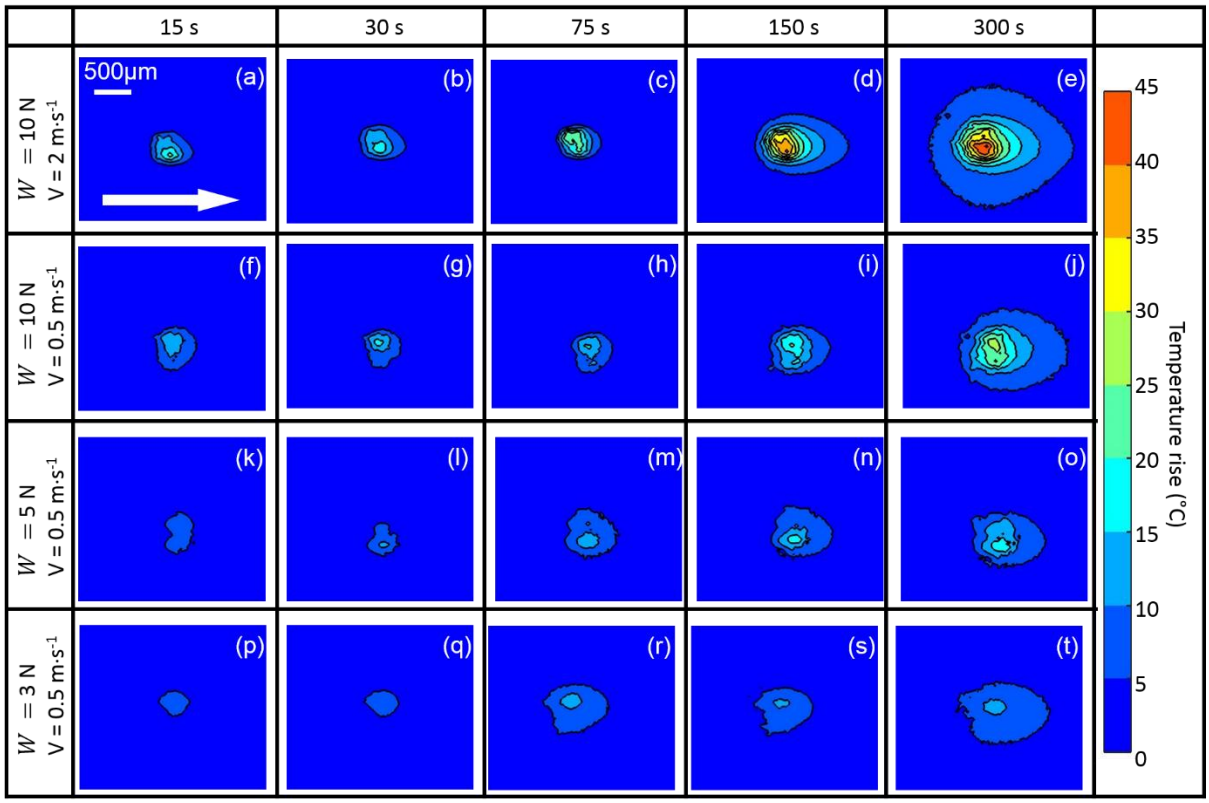

Figure 7 Temperature maps showing contact temperature rise ΔT_c at various applied loads when a stationary PBI ball was rubbed against a rotating sapphire. The sliding speed was (a) 2 m·s^{-1} and (b) – (d) 0.5 m·s^{-1}

The temperature maps (Figure 7) show the contact temperature rise ΔT_c varies with load and sliding speed. ΔT_c in the contact is not homogeneous: during the first 30 s, the heat distribution is roughly circular with only a small temperature variation in the contact. As the rubbing time increases, the temperature profile becomes increasingly asymmetric and both the average temperature rise ΔT_{ave} (Figure 8(a)) and the maximum temperature rise ΔT_{max} (Figure 8(b)) increase until they plateau. Whilst a hot zone develops in the contact, the trailing side (right) of the contact warms up. This is in agreement with the models by Blok and Jaeger [5-7, 44] which suggest that for Peclet numbers (Pe) above 5 (Pe is about 11 in this study) the location of maximum temperature moves towards the trailing edge of the contact, developing heat drag. A combination of high load, high velocity (Figure 7(a) – (e)) and poor thermal conductivity of PBI are responsible for the continuous increase of the contact temperature with rubbing time.

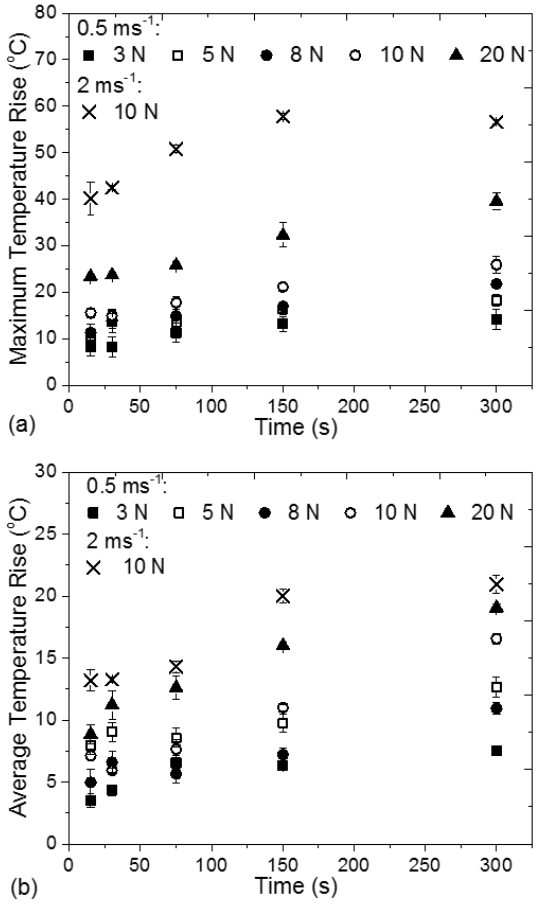

Figure 8(a) Maximum ΔT_{max} and (b) average contact temperature rise ΔT_{ave} at different loads and speeds against time. A stationary PBI ball was rubbed against a rotation sapphire disc at 0.5 m·s^{-1} for W= 3 – 20 N and at 2 m·s^{-1} for W= 10 N.

3.3.3. Linking applied load conditions with formation of a transfer layer

The results obtained at low loads, where the contact temperature rise is low, show that PBI transfers readily to steel at 280°C. Ex-situ observations of the wear scars show that the transferred material strongly adheres to the steel. In all cases, the polymer transfer layer initiates at the leading edge of the contact (Figures 6(a), (f) and (k)), suggesting the layer development is governed by the shear stresses in the contact, which are highest at the leading edge. The rest of the contact remains bare due to insufficient shear stress. In contrast, with increasing time (and therefore increasing contact temperature, as shown in Figure 8) the polymeric transferred material appears to initiate at the trailing edge, growing towards the leading edge of the contact. This appears to indicate that the growth in this case is temperature driven, as the contact temperature rise is the highest near the trailing edge (see Figure 7). This reduces the shear strength of the polymer at the rear of the contact and promotes polymer transfer from that location, towards the leading edge. The whole contact zone is eventually covered by the transfer layer. (Figures 6(b), (g) and (l))

Under high loading conditions the shear stress as well as the temperature rise in the entire contact are sufficiently high to cause continuous formation and removal of the transfer layer. As a result, only a very thin

and heterogeneous polymer transfer layer exists on the wear scar (see Figure 7(e)). Additionally, the polymer experiences a very high wear rate and a large amount of debris is produced.

A consequence of rubbing, likely due to the elevated contact temperature, is the increased growth of oxides on the steel surface (see Figure 4). The high stress, high temperature region in the contact has the thinnest oxide as they are rapidly removed. Note the oxides of the steel ball change from Fe_2O_3 in low load conditions to FeOOH in high load conditions which may impact on the potential formation of a transfer layer.

3.3.4. Linking applied load conditions with PBI friction and wear

Variations in contact pressure and contact temperature conditions for the high and low load cases give rise to different wear conditions. Under low load and low temperature conditions, the formation of a stable polymer transfer layer gives rise to a traditional 'protective mechanism': the developed layer adheres and covers the whole steel contact surface. The resulting PBI-PBI contact has a low friction coefficient (Figure 1(a)) and very low wear that is fairly independent of the actual thickness and morphology of the polymer layer.

Under high load conditions this protective mechanism fails: the temperature and shear stress in the contact are sufficiently high for any transfer layer to develop but also to be removed subsequently. The transfer layer undergoes this continuous cycle of removal and fast regeneration; as a result the polymer transfer layer on the steel ball is very thin and the wear rate of the PBI under these conditions is very high. Oxides, which grow more easily in these cases, may act as a third body and can be abrasive and thus contribute to increased wear for both steel and PBI as load (hence temperature) increases.

Despite the differences in transfer layer morphology in low and high load cases, the observed friction coefficients are independent of the applied load. This supports that only very thin PBI transfer layer on the steel surface is necessary for low friction steel-PBI contacts.

4. Conclusion

PBI is a high performance polymer with a high glass transition temperature, good mechanical properties and superior chemical inertness. It can be used at elevated temperatures that are unmatched by other polymers, which makes it an ideal candidate for high temperature tribological applications where lubricants cannot be used. In this work, we examined the tribological performance of PBI against steel at 280°C under non-lubricated, severe rubbing conditions using a steel ball against a PBI disc set-up. The amount of wear and the dominant wear mechanism of the PBI disc depend on the applied load. At low load conditions, the wear of the PBI disc is mild and occurs by ironing. When the load surpasses a critical value, the contact pairs wear until a critical value of the contact pressure is reached. At high load cases, cracks and pits are formed on the PBI wear tracks and both PBI and steel wear substantially.

There is a direct link between the temperature distribution inside the contact and the local formation of a polymer transfer layer. The morphology of the transfer layer is heterogeneous within the contact and is load dependent. At low load and low contact temperature conditions, a relatively thick PBI transfer layer rapidly develops on the steel surface. At high load and high contact temperature conditions, the majority of the contact

is covered by a very thin polymeric transfer layer due to the constant removal and regeneration of the transfer layer, giving rise to a high wear rate of the PBI. XPS results suggest that at low and high load conditions different iron oxides develop, α-Fe_2O_3 and α-FeOOH respectively. The change in surface chemistry may also contribute to differences in transfer film morphology and wear rate. The insensitivity of the measured friction in the steel-PBI contact to the applied load suggests that it is the existence rather than the morphology of the transfer layer that controls the friction.

For practical applications, one should be aware that, while PBI-steel contacts show low friction at high temperature conditions, under more severe loading (pressure and/or sliding velocity) conditions PBI can experience substantial wear. This is due to both high applied shear stress as well as elevated contact temperature from frictional heating. While the temperature rise does not necessary reach the glass transition or melting point of the polymer, a relatively small temperature rise may sufficiently lower the shear strength of the polymer strength. To mitigate such severe wear rates and the related failure of mechanical components, the implementation of an effective heat management strategy will be crucial to ensure that polymeric transferred materials on steel are not removed from the steel-PBI contact.

Acknowledgement

This work was supported by Hoerbiger UK Limited and EPSRC. The authors would like to thank Mr James Utama Surjadi for his help in conducting some of the friction and transfer layer thickness measurements. The authors gratefully acknowledge Dr Tom Reddyhoff for the use of his IR thermography setup.

Reference

[1] T.S. Chung, A critical review of polybenzimidazoles: Historical development and future R&D, Journal of Macromolecular Science-Reviews in Macromolecular Chemistry and Physics C37(2) (1997) 277-301.
[2] K. Friedrich, H.J. Sue, P. Liu, A.A. Almajid, Scratch resistance of high performance polymers, Tribology International 44(9) (2011) 1032-1046.
[3] M. Gruender, High-PV wear study of six high performance wear grade engineering plastics, NC: PBI Performance Products (2012).
[4] S. Sharma, E. Padenko, J. Bijwe, B. Wetzel, K. Friedrich, Erosive and sliding wear of polybenzimidazole at elevated temperatures, Journal of Materials Science 51(1) (2015) 262-270.
[5] J.C. Jaeger, Moving Sources of Heat and the Temperature at Sliding Contact, Journal and proceedings of the Royal Society of New South Wales 76 (1943) 203-224.
[6] H. Blok, The flash temperature concept, Wear 6(6) (1963) 483-494.
[7] J.F. Archard, R.A. Rowntree, The Temperature of Rubbing Bodies .2. The Distribution of Temperatures, Wear 128(1) (1988) 1-17.
[8] M.F. Ashby, J. Abulawi, H.S. Kong, Temperature Maps for Frictional Heating in Dry Sliding, Tribology Transactions 34(4) (1991) 577-587.
[9] G.M. Bartenev, V.V. Lavrentev, Friction and wear of polymers, Elsevier, Amsterdam, 1981.
[10] N.K. Myshkin, M.I. Petrokovets, A.V. Kovalev, Tribology of polymers: Adhesion, friction, wear, and mass-transfer, Tribology International 38(11-12) (2005) 910-921.
[11] B.L. Rees, Static friction of bulk polymers over a temperature range, Research (8) (1957) 331-338.
[12] K.V. Shooter, D. Tabor, The Frictional Properties of Plastics, Proceedings of the Physical Society. Section B 65(9) (1952) 661.

[13] W. Yanming, W. Tingmei, W. Qihua, Effect of molecular weight on tribological properties of thermosetting polyimide under high temperature, Tribology International 78 (2014) 47-59.
[14] H. Unal, M. Kurt, A. Mimaroglu, Tribological performance of industrial polyamide-imide and its composite under different cooling conditions, Journal of Polymer Engineering 32(3) (2012) 201-206.
[15] P. Samyn, P. De Baets, J. Van Craenenbroeck, F. Verpoort, G. Schoukens, Thermal transitions in polyimide transfer under sliding against steel, investigated by Raman spectroscopy and thermal analysis, Journal of Applied Polymer Science 101(3) (2006) 1407-1425.
[16] J.K. Lancaster, Abrasive wear of polymers, Wear 14(4) (1969) 223-239.
[17] B.J. Briscoe, S.K. Sinha, Wear of polymers, Proceedings of the Institution of Mechanical Engineers Part J-Journal of Engineering Tribology 216(J6) (2002) 401-413.
[18] B.J. Briscoe, C.M. Pooley, D. Tabor, Friction and Transfer of Some Polymers in Unlubricated Sliding, Abstracts of Papers of the American Chemical Society (1974) 33-33.
[19] S. Bahadur, C. Sunkara, Effect of transfer film structure, composition and bonding on the tribological behavior of polyphenylene sulfide filled with nano particles of TiO2, ZnO, CuO and SiC, Wear 258(9) (2005) 1411-1421.
[20] G.W. Stachowiak, A.W. Batchelor, 12 - Adhesion and Adhesive Wear, Engineering Tribology (Third Edition), Butterworth-Heinemann, Burlington, 2006, pp. 553-572.
[21] L. Chang, K. Friedrich, L. Ye, Study on the Transfer Film Layer in Sliding Contact Between Polymer Composites and Steel Disks Using Nanoindentation, Journal of Tribology-Transactions of the Asme 136(2) (2014).
[22] B. Briscoe, Wear of polymers- An essay on fundamental aspects, Tribology International 14(4) (1981) 231-243.
[23] S.H. Rhee, K.C. Ludema, Mechanisms of formation of polymeric transfer films, Wear 46(1) (1978) 231-240.
[24] S. Bahadur, The development of transfer layers and their role in polymer tribology, Wear 245(1–2) (2000) 92-99.
[25] R.L. Fusaro, Friction, Wear, Transfer, and Wear Surface Morphology of Ultrahigh-Molecular-Weight Polyethylene, A S L E Transactions 28(1) (1985) 1-10.
[26] K.A. Laux, C.J. Schwartz, Effects of contact pressure, molecular weight, and supplier on the wear behavior and transfer film of polyetheretherketone (PEEK), Wear 297(1-2) (2013) 919-925.
[27] J. Ye, H.S. Khare, D.L. Burris, Transfer film evolution and its role in promoting ultra-low wear of a PTFE nanocomposite, Wear 297(1-2) (2013) 1095-1102.
[28] D.H. Buckley, Friction and wear Characteristics of polyimide and filled polyimide compositions in vacuum, Nasa Technical Note (1966).
[29] K.A. Laux, C.J. Schwartz, Influence of linear reciprocating and multi-directional sliding on PEEK wear performance and transfer film formation, Wear 301(1-2) (2013) 727-734.
[30] R.L. Fusaro, Effect of Atmosphere and Temperature on Wear, Friction, and Transfer of Polyimide Films, A S L E Transactions 21(2) (1978) 125-133.
[31] P. Samyn, J. Quintelier, P. De Baets, G. Schoukens, Characterisation of polyimides under high-temperature sliding, Materials Letters 59(22) (2005) 2850-2857.
[32] Y.M. Wang, T.M. Wang, Q.H. Wang, Effect of molecular weight on tribological properties of thermosetting polyimide under high temperature, Tribology International 78 (2014) 47-59.
[33] J. Le Rouzic, T. Reddyhoff, Development of Infrared Microscopy for Measuring Asperity Contact Temperatures, Journal of Tribology 135(2) (2013) 021504-021504.
[34] K.G. Rowe, A.L. Bennett, B.A. Krick, W.G. Sawyer, In situ thermal measurements of sliding contacts, Tribology International 62 (2013) 208-214.
[35] K.A. Laux, A. Jean-Fulcrand, H.J. Sue, T. Bremner, J.S.S. Wong, The influence of surface properties on sliding contact temperature and friction for polyetheretherketone (PEEK), Polymer 103 (2016) 397-404.
[36] J.V. Voort, S. Bahadur, The growth and bonding on transfer film and the role of PTFE in the tribological behavior of PEEK, Wear 181 (1995) 212-221.

[37] P. Liu, M. Mullins, T. Bremner, J.A. Browne, H.J. Sue, Hygrothermal behavior of polybenzimidazole, Polymer 93 (2016) 88-98.
[38] G. Carbone, C. Putignano, A novel methodology to predict sliding and rolling friction of viscoelastic materials: Theory and experiments, Journal of the Mechanics and Physics of Solids 61(8) (2013) 1822-1834.
[39] A. Arvanitaki, B.J. Briscoe, M.J. Adams, S.A. Johnson, The Friction and Lubrication of elastomers, Tribology Series 30 (1995) 503-511.
[40] G. Bhargava, T.A. Ramanarayanan, I. Gouzman, E. Abelev, S.L. Bernasek, Inhibition of Iron Corrosion by Imidazole: An Electrochemical and Surface Science Study, Corrosion 65(5) (2009) 308-317.
[41] D.G. Chambaere, E. Degrave, The Beta-Feooh to Alpha-Fe2o3 Phase-Transformation - Structural and Magnetic Phenomena, Physics and Chemistry of Minerals 12(3) (1985) 176-184.
[42] N.W. Brooks, R.A. Duckett, J. Rose, I.M. Ward, J. Clements, An Nmr-Study of Absorbed Water in Polybenzimidazole, Polymer 34(19) (1993) 4038-4042.
[43] J.C. Pope, H.-J. Sue, T. Bremner, J. Blümel, High-temperature steam-treatment of PBI, PEEK, and PEKK polymers with H2O and D2O: A solid-state NMR study, Polymer 55(18) (2014) 4577-4585.
[44] G.W. Stachowiak, A.W. Batchelor, Chapter 7 - Elastohydrodynamic Lubrication, in: G.W. Stachowiak, A.W. Batchelor (Eds.), Engineering Tribology (Fourth Edition), Butterworth-Heinemann, Boston, 2014, pp. 293-370.
[45] R. Bassani, G. Levita, M. Meozzi, G. Palla, Friction and wear of epoxy resin on inox steel: remarks on the influence of velocity, load and induced thermal state, Wear 247(2) (2001) 125-132.

Graphic Abstract

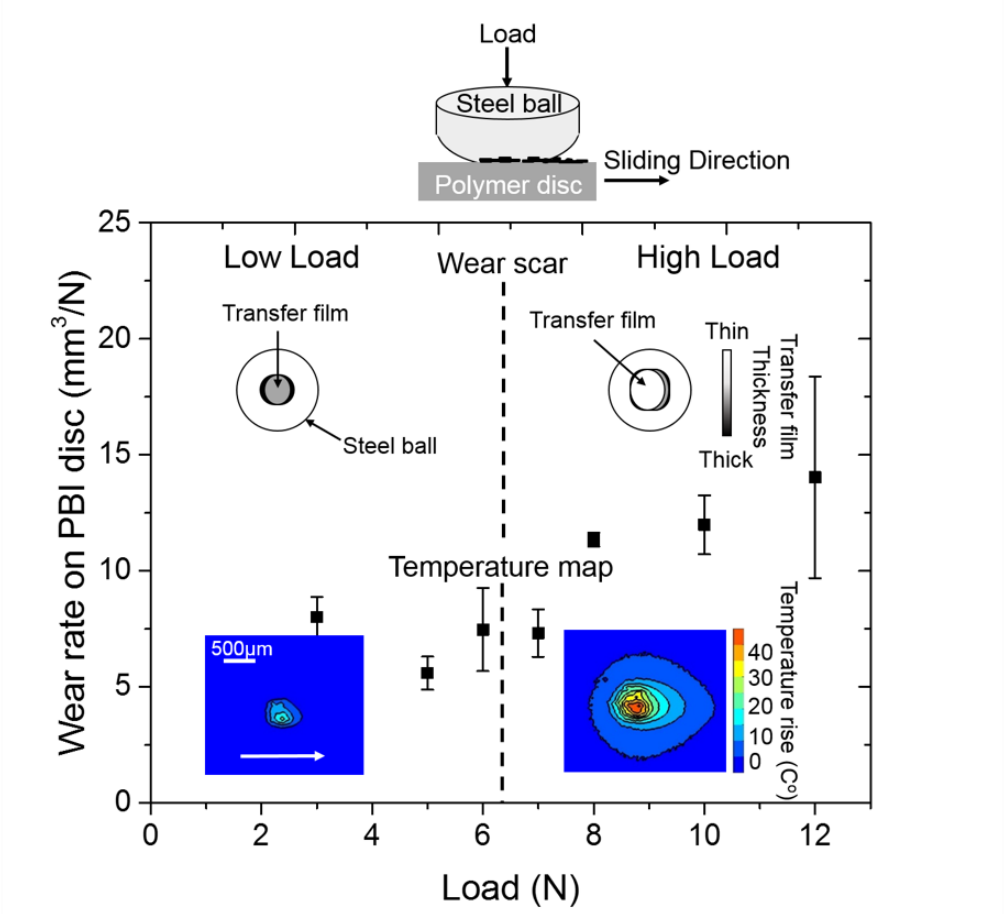

Highlight:

1. PBI has load independent friction but wear severity depends on load at 280°C.
2. PBI transfer film on steel controls friction and its morphology depends on load.
3. Contact temperature distribution governs transfer film distribution in contact.
4. High applied load causes high contact temperature and leads to high PBI wear.
5. To use PBI at severe rubbing conditions, contact temperature needs to be managed.